UDC 620
DOI: 10.15587/1729-4061.2022.267232

EFFECT OF SYZYGIUM CUMINI LEAF EXTRACT AS A GREEN CORROSION INHIBITOR ON API 5L CARBON STEEL IN 1M HCl

Rini Riastuti
Corresponding author
Doctor of Engineering, Senior Lecturer
Prof Johny Wahyuadi Laboratory*
E-mail: riastuti@metal.ui.ac.id
Giannisa Mashanafie
Master of Engineering*
Vika Rizkia
Doctor of Engineering**
Ahmad Maksum
Doctor of Engineering, Lecturer
Research Center for Eco-Friendly Technology**
Siska Prifiharni
Master of Metallurgical Engineering
Research Center for Metallurgy-National Research and Innovation Agency
KST B.J. Habibie, Tangerang Selatan, Indonesia, 15314
Agus Kaban
Master of Engineering, Graduate Student
Prof Johny Wahyuadi Laboratory***
***Department of Metallurgical and Materials Engineering
Universitas Indonesia
Kampus Baru UI Depok, Jawa Barat, Indonesia, 16424
Gadang Priyotomo
Doctor of Engineering
Research Center for Metallurgy-National Research and Innovation Agency
KST B.J. Habibie, Tangerang Selatan, Indonesia, 15314
Johny Soedarsono
Doctor of Engineering, Professor
Prof Johny Wahyuadi Laboratory***
*Department of Metallurgical and Materials Engineering
Universitas Indonesia
Kampus Baru UI Depok, Jawa Barat, Indonesia, 16424
**Department of Mechanical Engineering
Politeknik Negeri Jakarta
Jl. G.A. Siwabessy Kampus Baru UI, Depok, Indonesia, 16425

Corrosion in API 5L steel under 1M HCl is a common issue; hence, creating a more effective and naturally-based inhibitor is critical. In this research, Syzygium Cumini leaf extract (SCLE) was used as a new green corrosion inhibitor under acidic conditions. The inhibition properties of the novel cumini extract were thoroughly characterized using potentiodynamic polarization (PDP), electrochemical impedance spectroscopy (EIS), Fourier-transform infrared spectroscopy (FTIR), and atomic force microscope (AFM). The results show that the cumini inhibitor has excellent corrosion inhibition with 93 % inhibition efficiency. The adsorption behavior of the inhibitor follows the Langmuir Adsorption Isotherm due to the nearness of R^2 to unity. The potentiodynamic and electrochemical measurements demonstrate the mixed type of corrosion inhibitor. Thermodynamic calculation of ΔGads is − 18.41 kJ mol^{-1} showing the physical adsorption process between the inhibitor and metals. Further inspection of ΔHads at −58.93 kJ mol^{-1} considers releasing energy during adsorption. The FTIR results agree with the increased growth of passive layers due to the adsorption of polyphenol and flavonoids on metals. Remarkably, the adsorption peak at 3266.59 cm^{-1} corresponds to the adsorption of −OH. The peak at 1612.56 and 1698.4 cm^{-1} is attributed to C=C and C=O functional groups. The above functional groups serve as adsorption centers to reduce the corrosion effect. The surface treatment of AFM indicated a good relationship with the functional group characterization and confirmed the significant corrosion rate reduction. This work can be used as a benchmark to develop a natural plant as a corrosion inhibitor

Keywords: green corrosion inhibitor, Syzygium cumini leaf extract, physisorption, polyphenol and flavonoids based inhibitor molecules

Received date 05.09.2022
Accepted date 12.11.2022
Published date 30.12.2022

How to Cite: *Riastuti, R., Mashanafie, G., Rizkia, V., Maksum, A., Prifiharni, S., Kaban, A., Priyotomo, G., Soedarsono, J. (2022). Effect of syzygium cumini leaf extract as a green corrosion inhibitor on API 5L carbon steel in 1M HCl. Eastern-European Journal of Enterprise Technologies, 6 (8 (120)), 30–41. doi: https://doi.org/10.15587/1729-4061.2022.267232*

1. Introduction

Acids have been used in numerous industrial operations, including refining crude oil, pickling, cleaning, acid scaling, and petrochemical [1, 2]. Hydrochloric acid is the most extensively used among commercially available acids in the oil and gas industry, owing to its high solubility in the aqueous phase. It acidifies carbonates and removes scale, rust, and carbonite deposits [3–5]. However, hydrochloric acid might cause corrosion in a metallic material and is highly destructive [6, 7]. Adding corrosion inhibitors is one of the most practical and convenient ways to protect the metal from corrosion attacks. A corrosion inhibitor is a substance that, when introduced in low quantities to a corrosive environment, effectively reduces or suppresses the corrosion of metal in an acidic medium [8–10]. It reduces the rate of metal dissolution by adsorbing ions or molecules to form a protective layer on the metal [11].

Various chromates, silicates, phosphates, and arsenate-based inorganic inhibitors were offered as high-performance inhibitors; nevertheless, their usage is restricted

by numerous environmental laws [12]. Synthetic organic inhibitors were also developed in the past; however, their toxicity level and manufacturing cost limit their use [13]. Therefore, researchers focused on developing eco-friendly, inexpensive, and biodegradable corrosion inhibitors [14, 15]. In the existing development of inhibitors, various sources generated from biopolymers [16], ionic liquids [17], and plant extract [18] have been invented and developed to suppress aggressive acidic solutions.

With this in mind, the shifting to harness the potential of green inhibitors provides several benefits, such as high accessibility, ease of production, renewability, and effectiveness [19, 20]. The inhibitive property of plant extracts is ascribed to active organic compounds containing nitrogen, oxygen, and sulfur heteroatoms, as well as C–C bonds with π electrons that interact with vacant metal d-orbitals [20, 21]. This work attempts to resolve the use of leaf extract from *Syzygium Cumini*, which might be a potential candidate to become a natural corrosion inhibitor due to its biodegradability and high solubility in water. Unfortunately, there is little discussion, such as the procedure to prepare the inhibitor, type of adsorption, and surface modification, which become an obstacle to commercializing the inhibitor. Therefore, the study requires research to unveil the potential of *Syzygium Cumini* as a green corrosion inhibitor.

2. Literature review and problem statement

Several publications related to developing a part of a natural plant as an inhibitor have recently provided better insight, including using leaves. The study conducted in [22] shows that the combination between piper beetle and green tea is suitable to interrupt the corrosion rate of API X-52 steel in the aerated 3.5 % NaCl solution. The other publication [23] uses *Chrysanthemum Coronarium* leaves to increase the evolution thickness of the protective film on the aluminum surface. The film raises the electrostatic interaction between the hydrogen bonds and their combinations of aluminum metals and the inhibitors. In addition, the work [24] provides a clear explanation of how the *Date* palm leaf extract protects the X60 carbon steel under 15 wt % HCl solution. They reported that the inhibitor depresses the corrosion rate to nearly 82 % at 60 °C. Moreover, the study [25] shows the extract of *Pluchea indica* to investigate the corrosion resistance of the inhibitor, which appears as a mixed-type inhibitor. The work reveals that the solution effectively protects carbon steel for nearly 220 hours due to the contribution of its functional groups.

It is shown that corrosion involves interaction between the metal, electrolyte, and electrochemical potential, which can be mitigated by controlling one of the above parameters. But the unresolved issue is related to disconnecting the conjunction using a corrosion inhibitor and conducting its corresponding testing as a key to process newly developed corrosion inhibitors. The reason can be determining the corrosion resistance performance of the coated materials by exposing them to a corrosive solution, which makes the corresponding research inexpedient.

An option to overcome the relevant difficulties can be extracting dominant essential molecules from plant leaves to inhibit the electrochemical process. The approach used in the *Bauhinia Tomentosa* leaf extract [8] is an example of a suitable corrosion inhibitor for steel with inhibition efficiency beyond 90 %. According to their report, an increasing concentration in the temperature range of 308–323 K raises the resistance of charge transfer while depressing the double-layer capacitance. The extract of *Centipeda Minima* [26] has provided an inhibition property of about 96.2 % using 500 mg/L inhibitor solution. The uniqueness of the prepared inhibitor shows the extraction of facile hot water, and the freeze-drying process has successfully given superior inhibition to protect carbon steel under hydrochloric acid solution. In addition, the study [27] shows that an equal concentration of sodium dichromate and *Solanum aethiopicum* leaf extract at 0.83 % chemically protected the steel-rebar corrosion activity. In this study, the phytochemical results indicate that the leaf extract fits the green concept of environmentally and eco-friendly inhibitors.

In this work, utilizing the *Syzygium cumini* leaf extract is an attractive possibility because it would provide a better insight into corrosion mitigation with minimal or no hazardous effect. Specifically, the study attempts to test the inhibition activity to identify the most influential functional groups and their contribution under aggressive acidic solutions. The previous work [28] unveiled that the phenolic content of natural inhibitors is water soluble, and protonated functional groups such as –OH, C–O–C, C=O, and Aryl–CH_3 in their structure give higher solubility in water. The inhibitor adsorption model shows the quantitative and qualitative relationship between the inhibitor molecules and bare metals. From the surface modification point of view, the adsorbed inhibitor smoothens the damaged surface, especially when metal is immersed within a time frame to estimate the corrosion resistance of the prepared inhibitor.

Particularly, this work considers using the *Syzygium Cumini* leaf extract to protect the API 5L carbon steel related to the corresponding inhibition action, thermodynamics, and surface studies. It includes the effect of inhibitors when the metal was immersed for some time and tested for their inhibitory activity. The latter objective was not detailed in the above publications.

All this allows us to argue that it is appropriate to conduct a study devoted to revealing the effectiveness of *Syzygium cumini* in controlling corrosion scenarios.

3. The aim and objectives of the study

The study aims to provide the anticorrosive *Syzygium Cumini* leaf extract (SCLE) as a new corrosion inhibitor. This will enable injecting the inhibitor into oil pipelines to improve corrosion resistance under low pH environments.

To achieve this aim, the following objectives are accomplished:

– to characterize the associated inhibitor functional group in increasing the anti-corrosion activity, including the immersion time of adsorption;

– to evaluate the effect of temperature on the considerable adsorption behavior of inhibitors related to their thermal stability;

– to compare the surface treatment in the absence and presence of the *Syzygium Cumini* leaf inhibitor.

4. Materials and methods

4. 1. Object and hypotheses of the study

The object of this study is *Syzygium Cumini* leaves taken from Jakarta, Indonesia. Before processing the

inhibitor, the leaves were cleaned, dried, and crushed to increase the extraction surface area. It is assumed that the leaf extract's phenolic and amine compounds increase the inhibitor's thermal stability and reduce the corroded area. It is also hypothesized that the conjugation of C=C, C=O, –OH, –NH, and the inhibitor's heteroatoms groups involves the mitigation of corrosion through the formation of chemical bonding. It is also presumed that the inhibitor concentration affects its effectiveness during the immersion period of metals.

4. 2. Inhibitor solution and materials

Dried *Syzygium cumini* leaf powder was weighed and soaked in 70 % ethanol before further refluxing was conducted. Dilute 1M HCl (blank solution) was prepared from diluting 37 % HCl solution (Merck. Co) before mixing the inhibitor solution to prepare 100, 200, 300, 400, and 500 ppm test solutions. The composition of the API 5L specimen was C: 0.064 %, Si: 0.130 %, Mn: 0.766 %, P: 0.015 %, S: 0.004 %, Cr: 0.002 %, Mo: 0.001 %, Ni: 0.009 %, Ti: 0.001 %, Cu: 0.019 %, Nb: 0.013 %, Al: 0.028 % and the rest is Fe. The ASTM G5-14 was implemented for the specimen pre-treatment. The prepared specimen dimensions were 10×10 mm, and it was abraded using silicon carbide paper of various grades spanning 400–1,200. Before the electrochemical test, the prepared metal was rinsed with distilled water, degreased with acetone, and dried.

4. 3. Anticorrosion inhibitor test

Electrochemical impedance spectrometry (EIS) and Potentiodynamic polarization measurements were conducted using the Gamry Potentiostat Corrosion Measurement System (CMS). In detail, the API 5L serves as a working electrode, while a platinum wire was used as a counter electrode. In addition, a saturated calomel electrode was selected as a reference electrode. A comparable steady status was attained by immersing the working electrode in the test solution to achieve OCP (open circuit potential) for one hour. The EIS test was executed upon receiving the OCP-tested data. On the other hand, the perturbation signal was set at the selected frequency range of 300,000–0.1 Hz using the amplitude of AC signals at 10 mV. In addition, the potentiodynamic polarization curves were conducted using a scan rate of 5 mV with a potential range of –250 to +250 mV vs. OCP.

4. 4. Identification of a functional group and surface analysis of inhibitors

Fourier-Transform Infrared (FTIR) spectra were collected using the ASTM E1944 standard to unveil the functional group of the inhibitor extract, including identifying the adsorbed compound over the surface of the working electrode. The spectrum range was 400–4,000 cm^{-1} with 64 scan numbers. The surface characterization was characterized using Atomic Force Microscope (AFM) by immersing the mild steel with and without a 500 ppm SCLE inhibitor.

5. Results of the study of Syzygium Cumini leaves as green corrosion inhibitors

5. 1. Anti-corrosion activity of the inhibitor

The potentiodynamic polarization technique was conducted to study the API 5L polarization response in 1 M HCl with the addition of various concentrations of SCLE. Fig. 1 shows the Tafel polarization curves of the working electrode immersed in the SCLE inhibitor at concentrations of 100, 200, 300, 400, and 500 ppm, including the blank solution measured at 30–50 °C. The electrochemical parameters entail corrosion current density (i_{corr}), corrosion potential (E_{corr}), anodic and cathodic Tafel slope (β_a and β_c), and inhibition efficiency (η).

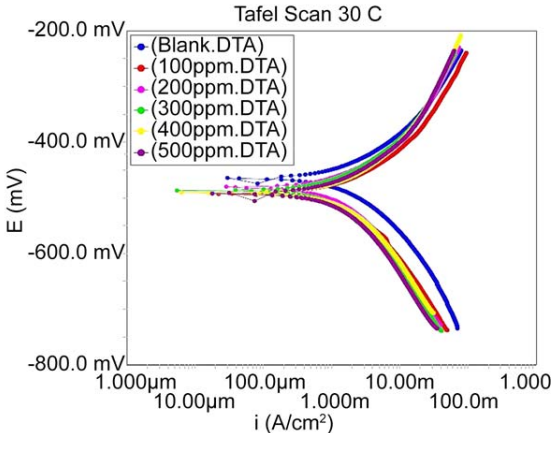

a

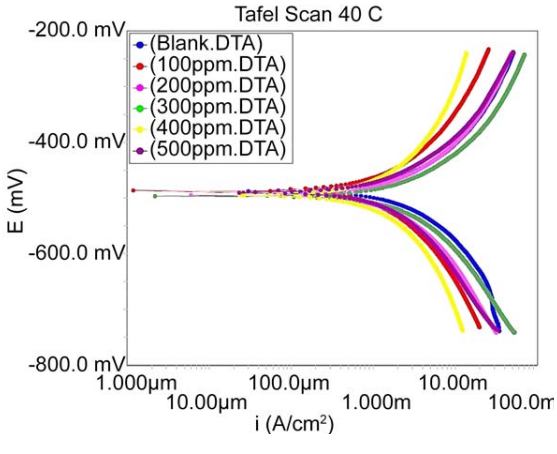

b

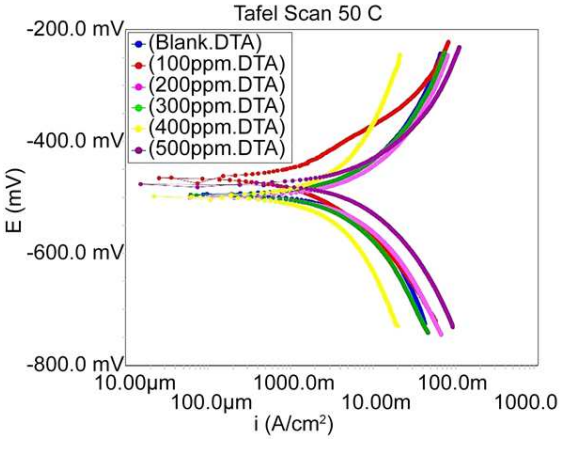

c

Fig. 1. Results of anti-corrosion behavior: *a* – 30 °C; *b* – 40 °C; *c* – 50 °C

Fig. 1 illustrates that the anodic and cathodic branches of the Tafel curves shift to a lower current density after the addition of inhibitors. In the inhibited working electrode, the corrosion potential, E_{corr}, shifted towards the negative region/branch at all the studied temperatures (Fig. 1). On the other hand, the corrosion current density (i_{corr}) shows depression when the inhibitor is added to the test solution. The results of calculated E_{corr} and i_{corr} equally indicate the corrosion protection of the inhibitor. It is also important to note that the shape of the anodic and cathodic regions is similar except for the graph at 50 °C, which exhibits a little deviation at 400 ppm solution.

Table 1 shows the results of some electrochemical parameters E_{corr}, i_{corr}, β_a, β_c and η to obtain more details about the corrosion process, including the calculation of inhibition efficiency, η, using (1) as shown below:

$$\left\{\eta = \frac{i^0_{corr} - i_{corr}}{i^0_{corr}} \times 100\,\%\right\}. \quad (1)$$

In the above equation, i^0_{corr} and i_{corr} are corrosion current densities in the absence and presence of inhibitors.

Table 1

Calculated polarization parameters of the test solution in the medium at different inhibitor concentrations and temperatures

T (°C)	$C_{inhibitor}$ (ppm)	β_a (mV/dec)	β_c (mV/dec)	i_{corr} (mA/cm^2)	E_{corr} (mV)	*Corr rate* (mmpy)	η (%)
30	0	124.0	149	3.43	−465	39.84	0 %
	100	96.4	139	1.47	−493	17.10	57 %
	200	93.8	150	1.29	−481	15.02	62 %
	300	94.5	142	1.16	−487	13.52	66 %
	400	88.0	115	1.09	−491	12.68	68 %
	500	59.0	81	0.385	−492	4.167	90 %
40	0	225	240	4.8	−487	55.85	0 %
	100	124	156	2.95	−486	34.28	39 %
	200	152	212	2.51	−495	29.17	48 %
	300	150	193	3.21	−497	26.67	52 %
	400	256	258	2.13	−495	24.75	56 %
	500	117	159	1.54	−490	17.87	68 %
50	0	219	274	7.4	−494	86.17	0 %
	100	128	143	5.08	−471	59.15	31 %
	200	134	157	4.67	−500	54.31	37 %
	300	138	195	4.14	−496	48.06	44 %
	400	253	251	3.34	−499	38.86	55 %
	500	205	211	2.68	−499	31.18	64 %

Table 1 agrees with Fig. 1 to show that the presence of the inhibitor alters the anodic and cathodic curves in lowering the current density values (i_{corr}). The finding is particularly significant showing that increasing the concentration of inhibitor to 500 ppm improves the API 5L's corrosion resistance by dramatically lowering the i_{corr} value. The highest efficiency values obtained at 30, 40, and 50 °C are 90 %, 68 %, and 64 %, respectively. The results of Table 1 indicated that an increase in temperature raises i_{corr} (0.385 mA/cm^2, 1.54 mA/cm^2, and 2.68 mA/cm^2) and the corresponding corrosion rate, resulting in a decrease in inhibitor efficiency.

Fig. 2 shows the Nyquist spectra of the impedance of blank solution and various inhibitor concentrations in the range of 100–500 pm at a measured temperature of 30–50 °C.

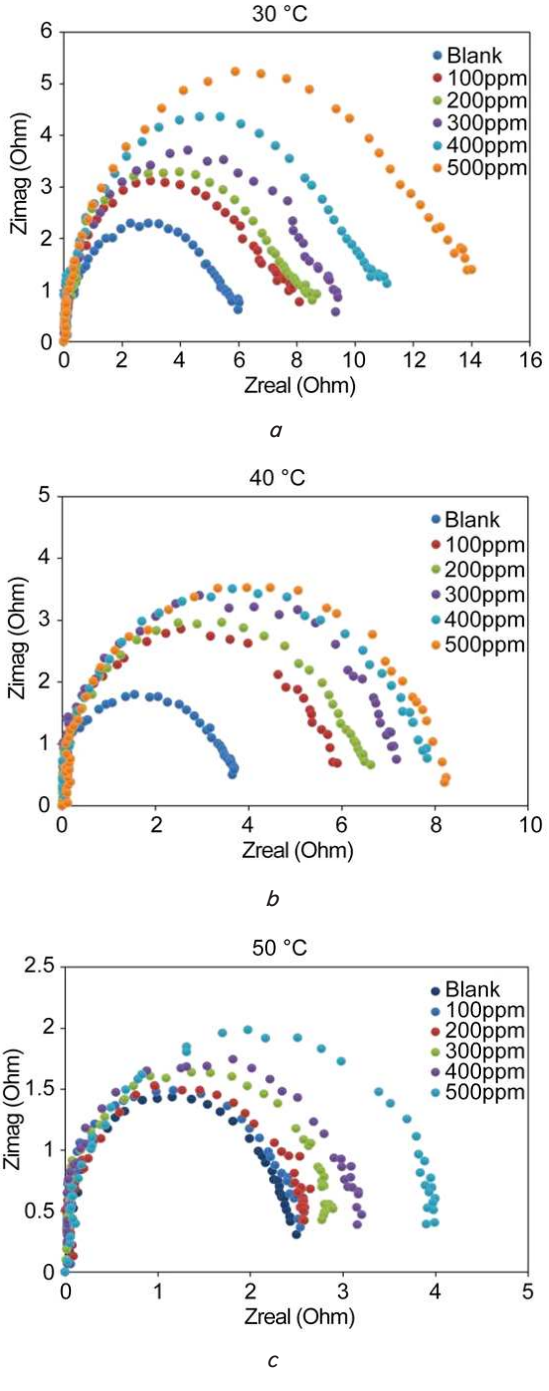

Fig. 2. Nyquist Plot of the inhibitor test solution at various temperatures: *a* — 30 °C; *b* — 40 °C; *c* — 50 °C

It is essential to note from Fig. 2 that single depressed semicircles for all temperatures appear. Careful observation of the graph shows that the diameter of the semicircles increases in the inhibited solution compared to without the inhibitor. Despite a similar trend, the effect of higher temperature limits the inhibitor protection as the diameter of the semicircle decreases. The capacitive loops for all temperatures are identical and slightly concave to show the increasing surface heterogeneity of the working electrode [29]. The imperfect single plot reveals that the inhibition process has one relaxation time constant to a growing frequency dispersion effect [30].

The length of the Nyquist diameter is inseparable from the inhibition efficiency (η). The calculation of η is shown in (2) [31]:

$$\left\{\eta((\%)=\frac{R_{ct}-R_{ct}^{0}}{R_{ct}}\times 100\,\%\right\}. \quad (2)$$

In the above equation, R_{ct}^{0} and R_{ct} are the charge transfer resistance of the bare electrode and the inhibitor.

Table 2 shows the electrochemical impedance spectroscopy results of the inhibitor spans from 30–50 °C.

Table 2

Electrochemical parameters from the EIS fitting results at different concentrations and temperatures

T (°C)	$C_{inhibitor}$ (ppm)	R_{ct} (Ω)	R_s (Ω)	C_{dl} (μF)	η (%)
30	0	3.271	1.656	79.90	–
	100	5.681	1.373	77.50	42.4
	200	7.129	1.881	73.60	54.1
	300	9.019	1.358	69.40	63.7
	400	9.907	1.584	62.50	67.0
	500	12.63	1.308	60.90	74.1
40	0	3.318	0.604	103.70	–
	100	4.792	1.221	101.90	30.8
	200	6.180	1.401	99.97	46.3
	300	6.805	1.237	99.73	51.2
	400	7.368	1.302	98.99	55.0
	500	8.612	1.154	98.54	61.5
50	0	1.924	1.001	162.7	–
	100	2.251	0.829	149.0	14.5
	200	2.463	1.243	138.0	21.9
	300	2.676	1.093	131.0	28.1
	400	2.926	1.14	127.3	34.2
	500	3.157	1.213	124.7	39.1

According to the impedance results in Table 2, the charge transfer resistance (R_{ct}) value rises as the SCLE inhibitor concentration increases. It is noteworthy to compare that the remarkable rise of R_{ct} at 30 °C is smaller than at higher temperatures. The highest protection given by the EIS test was 74.1 % and 61.5 % at 30 and 40 °C. When the experiment continues to reach the temperature of 50 °C, the charge transfer resistance drops with 500 ppm solution. The gradual decrease of R_{ct} was observed at 50 °C to show a downward trend in transferring an electron from the inhibitor to the working electrode. Likewise, as the concentration of SCLE increases, the value of the double-layer capacitance (C_{dl}) decreases. The lowest value of C_{dl} is 60.90 μF, which refers to the corrosion protection of the inhibitor. It is also reported that at higher temperatures, the inhibitor protection achieves a lower value of η at 39.1 %.

The results of EIS align with the electrical equivalent diagram, as depicted in Fig. 3.

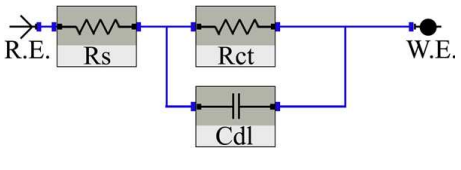

Fig. 3. Proposed electrical equivalent diagram

Fig. 3 represents the fitting impedance spectrum (based on Randles equivalent circuit model) that entails solution resistance (R_s), charge transfer resistance (R_{ct}), and C_{dl} of double-layer capacitance to model the corrosion mitigation of the inhibitor at different temperatures and concentrations.

Fig. 4 shows the effect of immersion of metals in the inhibitor solution within 0–60 mins to provide an insight into the protection capability using a 500 ppm solution.

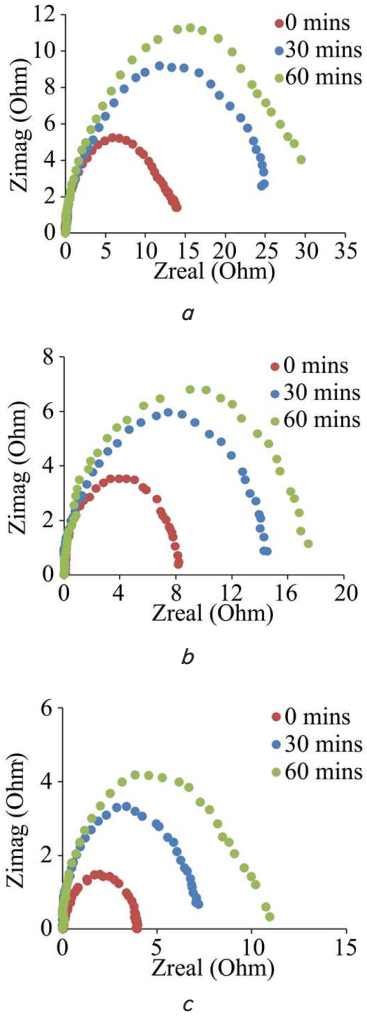

Fig. 4. Effect of immersion time: *a* – 30 °C; *b* – 40 °C; *c* – 50 °C

As shown in Fig. 4, only one semicircle Nyquist single depression graph is seen and increases with the immersion time. However, the diameter at higher temperatures is shorter than at lower temperatures. The recorded maximum protection of metal is 30 Ω at 30 °C (Fig. 4, *a*). It is also revealed that the semi-arc shape of the Nyquist spectra does not change remarkably, and each temperature measurement gives the same shape [32]. It is also obvious in Fig. 4 that the Nyquist plots are somewhat oblate after 60 min immersion time at all measured temperatures, which confirms the result of the electrochemical parameter as depicted in Table 4.

Table 4 illustrates the results of electrochemical measurement with 500 ppm inhibitor solution at various immersion times and temperature ranges. It can be reported that the inhibitor achieves maximum protection for 1 hour in all observable measurements. The values of R_{ct} and C_{dl} at 30 °C

are 27.43 Ω and 53.20 μF to give an inhibition efficiency of 54.1 %. Likewise, the inhibitor gradually lost its protection at 50 °C to give lower charge transfer resistance and a capacitive double layer at 8.444 Ω and 113.70. Hence, it can be concluded that a single dose of inhibitor injection into the test solution interrupts the electrochemical activity [33].

Table 4

Electrochemical parameters of API 5L obtained from immersion in 1 M HCl solution containing 500 ppm SCLE at various temperatures and immersion time

$C_{inhibitor}$ (ppm)	T (°C)	Immersion time (min)	R_{ct} (Ω)	R_s (Ω)	C_{dl} (μF)	η (%)
500	30	0	12.63	1.308	6090	0
		30	20.18	1.468	55.60	42.4
		60	27.43	1.750	53.20	54.1
	40	0	8.612	1.154	98.54	0
		30	12.26	1.146	93.54	30.8
		60	16.67	1.315	91.62	46.3
	50	0	3.157	1.213	124.70	0
		30	6.502	1.057	114.30	14.5
		60	8.444	1.201	113.70	39.1

The above results correlate with the adsorption of several functional groups from the inhibitor to the steel surface. Fig. 5 provides the results of FTIR to delve into more profound insight into the actual molecules involved in the inhibition reaction.

Fig. 5 unveils several absorption peaks related to the increase in the corrosion resistance of inhibitors. The broad absorption peak at 3266.59 cm^{-1} is attributed to –OH and –NH stretching vibration [34]. The band appears at 2933.85 cm^{-1}, referring to C–H stretching vibration and $>CH_2$ associated with saturated aliphatic groups (alkenes). The peak at a wavenumber of 1447.64 cm^{-1} indicates the C–H bond. The absorption peaks at 1219.06 and 1041.61 are related to C–O stretching vibration. Meanwhile, the absorption peaks at 1612.56 and 1698.4 cm^{-1} indicate the presence of C=C and C=O groups, respectively.

5. 2. Effect of temperature on the inhibitor adsorption

The adsorption isotherm models the mechanism of inhibitor over the mild steel surface; the results are shown in Fig. 6. Adsorption isotherm modeling is essential to determine the mechanism of interaction involved in the adsorption of inhibitor molecules onto the metal surface [35]. Several models, such as Langmuir isotherm, can be used to describe the adsorption mechanism involved. The calculated model is given by plotting a graph between concentration (C_{inh}) and concentration versus surface coverage (C_{inh}/θ) as depicted in Fig. 6. The surface coverage (θ) of API 5L as a function of the inhibitor concentration was calculated using (3) [36]:

$$\left\{\frac{C_{inh}}{\theta}=\frac{1}{K_{ads}}+C_{inh}\right\}. \quad (3)$$

The above equation shows K_{ads} as the adsorption-desorption constant (ppm^{-1}).

Fig. 6 shows that the linear correlation coefficient (R^2) values approach near unity (0.9993, 0.9922, and 0.9703 for 30, 40, and 50 °C, respectively), indicating that the inhibitor adsorption follows the Langmuir isotherm. Furthermore, the relationship between K_{ads} and ΔG_{ads} is given in (4):

$$\left\{\Delta G^0_{ads}=-RT\ln\left(10^6 K_{ads}\right)\right\}, \quad (4)$$

where the R is a gas constant of 8.31 kJ/mol and T is the absolute temperature (K). On the one hand, the calculated thermodynamic value of ΔG_{ads} shows the feasibility of the adsorption process and is intended to unveil the nature of inhibition. On the other hand, the relationship between ΔG_{ads}, ΔH_{ads}, and ΔS_{ads} is provided in (5):

$$\left\{\Delta G^0_{ads}=\Delta H^0_{ads}-T\Delta S^0_{ads}\right\}. \quad (5)$$

In the above equation, ΔH_{ads} is the enthalpy change of adsorption, and ΔS_{ads} is the entropy of adsorption. Both parameters are measured in kJ/mol.

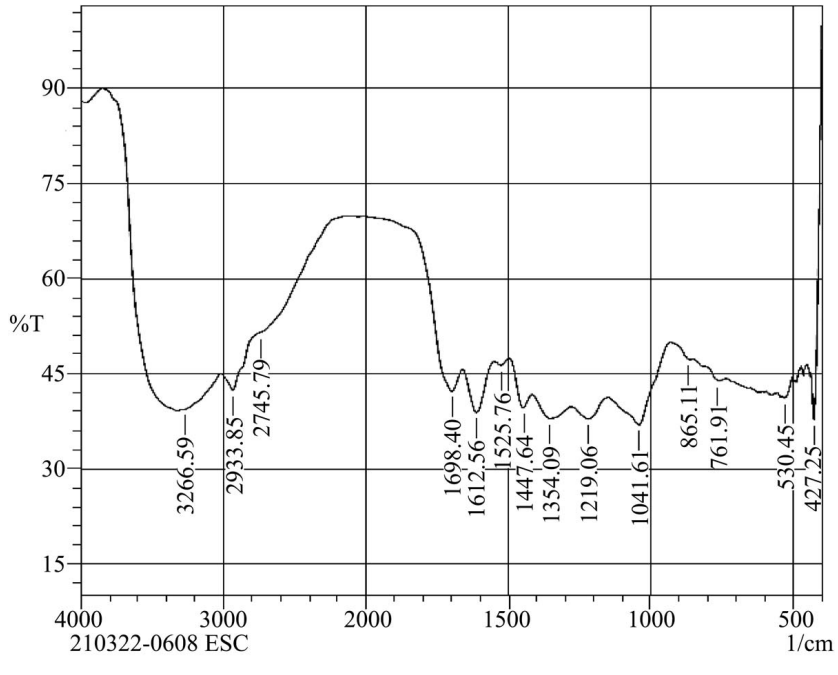

Fig. 5. Fourier-Transform Infrared spectra of the Syzygium Cumini leaf extract

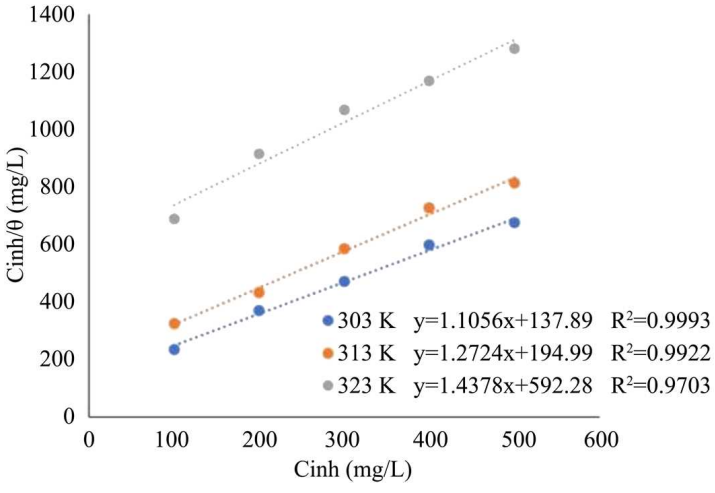

Fig. 6. Langmuir adsorption isotherm plot of API 5L in 1M HCl with the addition of various concentrations of inhibitor

The enthalpy change of adsorption was calculated using (6),

$$\ln K_{ads} = \ln \frac{1}{C_{solvent}} - \frac{\Delta H^0_{ads}}{RT} + \frac{\Delta S^0_{ads}}{R}. \quad (6)$$

Table 5 shows the obtained values of thermodynamic parameters of the inhibitor solution at various temperatures.

It is evident that the value of ΔG_{ads} is more remarkable than −40 kJ/mol, which defines the physisorption in nature (Table 5). The value of ΔH_{ads} at 323 K shows that the adsorption process releases energy (exothermic). The higher value of ΔS_{ads} shows the feasibility and spontaneity of the reaction from liquid to adsorbed monolayer inhibitor at −119.51 kJ/mol.

Table 5

Calculated thermodynamic parameters of the inhibitor at various temperatures

Temp (K)	K_{ads} (ppm^{-1})	ΔG_{ads} (kJ/mol)	ΔH_{ads} (kJ/mol)	ΔS_{ads}s (kJ/mol)
303	0.0073	−22.02	−58.93	−119.51
313	0.0051	−21.16	−58.93	−119.51
323	0.0017	−18.41	−58.93	−119.51

5. 3. Surface modification studies

The Atomic Force Microscope (AFM) was utilized to examine untreated (blank solution) and treated metals immersed in the 500 ppm inhibitor at 30 °C (Fig. 7).

It can be seen that the surface of API 5L was irregular and had heavy damage in the absence of the SCLE inhibitor, implying that the API 5L surface had been strongly corroded (Fig. 7, *a*, *b*). On the contrary, the surface in the presence of 500 ppm SCLE inhibitor at 30 °C was smoother (Fig. 7, *b*, *c*). This is confirmed by the value of the skewness parameter at 0.06101 nm, which is smaller before immersing mild steel in 1M HCl (0.4080 nm).

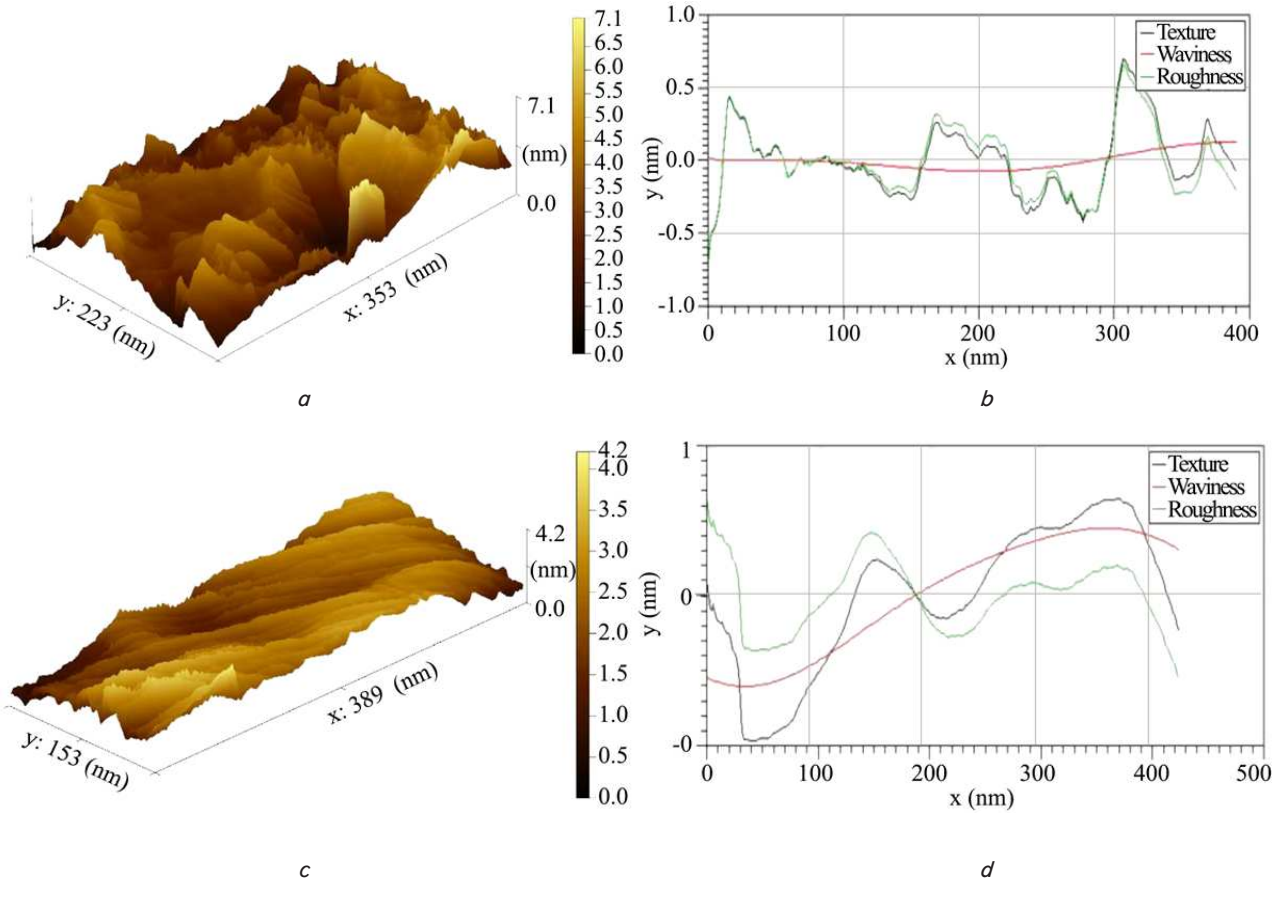

Fig. 7. Atomic force microscopy results of: *a* — uninhibited 3D plot; *b* — 2D uninhibited representation plot; *c* — inhibited 3D plot; *d* — 2D inhibited representation plot

6. Discussion of *Syzygium Cumini* as a green corrosion inhibitor

The anti-corrosion study of the *Syzygium Cumini* inhibitor was characterized using potentiodynamic polarization and electrochemical impedance spectroscopy. The Tafel polarization curves show that both cathodic and anodic curves displaced toward the negative and positive corrosion potential. The displacement indicates that SCLE acts as a mixed-type inhibitor that hinders both anodic and cathodic reactive sites due to the electroactive components of the inhibitor being adsorbed across the API 5L surface [37, 38]. In addition, shifting potential corrosion is less than −85 mV from the blank to the anodic or cathodic directions; inhibitors can be classified as mixed-type inhibitors [39, 40]. The displacement of potential corrosion was all less than −85 mV. It shows that SCLE is a mixed-type inhibitor for all the studied temperatures.

Based on Fig. 1 and Table 1, in the presence of the inhibitor, both anodic and cathodic curves were altered to the lower current density values (i_{corr}). The decrease in i_{corr} due to the adsorbed phytochemical components of SCLE on the API 5L surface hindered both anodic and cathodic active sites. This indicates that a blocking mechanism exists by the phenolic compounds in the cathodic region by reducing the rate of hydrogen ions to accept electrons [41]. Simultaneously, a donor-acceptor mechanism occurs in the anodic region, in which the SCLE compounds move actively to donate free electrons into the vacant orbit of the metal atom. The decrease in i_{corr} leads to the reduction of the corrosion rate. The phenomenon can be ascribed to the increasing rate of solubility of the metal and partial desorption of inhibitor molecules on the metal surface. Furthermore, the protective film formed is unstable, and the inhibition ability is weakened [42].

The EIS results show the appearance of a single depressed semicircle to indicate that the charge transfer mechanism controlled the corrosion processes [43]. As depicted in the Nyquist plot, the larger the diameter, the higher the charge resistance, making the metal less likely to be corroded [44]. Increasing the concentration of SCLE raises the absorption into the API 5L surface, which leads to the improvement of surface coverage and protection of the API 5L surface. Fig. 2 shows that due to the effectiveness of the protective film, the addition of an inhibitor only increases the impedance value, which is demonstrated by the similar shape between the absence and presence of SCLE addition [45].

On the contrary, the high-temperature effect decreases the semicircle curve diameter in the high-frequency area. This behavior implies that high temperatures accelerated corrosion. The addition of SCLE shows that the diameter of the semicircle retains the same length as the blank condition, demonstrating that SCLE has remarkable corrosion inhibition at high temperatures. The Nyquist plots are interpreted using a fitting line to determine the Randles equivalent circuit model. According to the impedance results, the higher charge transfer resistance is associated with the adsorption of inhibitors by blocking numerous active sites on the corroded materials [46].

The inverse influence of double-layer capacitance appears when the concentration of the inhibitor is increased. There are a few considerations to the following fact:

– the replacement of ions or water molecules with SCLE inhibitor organic molecules;

– an increase in the thickness of the electrical double layer at the electrode-electrolyte interface;

– a minor in the electroactive area, as reported in [47].

As a result, the C_{dl} value is gradually lowered since a more incredible solidification process occurred when the inhibitor was added.

The effect of temperatures provides the key to revealing inhibitor thermal stability at various temperatures. The lower value of R_{ct} is obtained when the temperature increases to show the metal's higher dissolution rate and the inhibitor's desorption at elevated temperatures [48]. The result of immersion time (Fig. 4) agrees well with the variation of temperature at a given range. Table 1 agrees with Table 2 in terms of the value of inhibition efficiency. Although it is a lower value at a higher concentration, the inhibitor remains stable to protect the metal from corrosion. However, to elevate any inhibition efficiency at a higher temperature, the addition of a natural phenolic and amine-based inhibitor is required to establish more hydrogen bonds and promote a chemical bond between metals and the inhibitor.

The immersion time defines the period frame where the adsorbed molecules are solidified on the surface of metals. In this work, the intention of modeling the effect of immersion time is to determine the performance of a single inhibitor dose. Based on Fig. 4, the longer residence time induces the formation of a thicker film due to more inhibitor molecules adsorbed on the metal surface. It is also noteworthy that increasing immersion time enlarges the diameter of the Nyquist curve's semicircle. The phenomenon corresponds to the adsorption of inhibitor molecules at the metal/solution interface, forming a time-stable protective layer [49].

Fig. 5 shows the result of the active functional groups involved in the adsorption, which is considerably related to the declining corrosion rate of the studied materials. Considering the functional group identified in the preceding section, the appearance of –OH and –NH induces the hydrogen bonding between the inhibitor molecules and the negative charge of the metallic surface [50]. The associate C=C and C=O enrich the adsorption process by extending the electron conjugation in *p*-orbital and lone pair of electrons in oxygen atoms. The same result was reported by [51]. In comparison, the rest of identified atoms and functional groups contribute to increasing the feasibility of the reaction, which is carefully inspected in the thermodynamic values of inhibition.

According to Table 5, the lower value of ΔG_{ads} corresponds to the formation of chemical bonding of dative covalent bonds. The fact confirmed in Fig. 6 is that chemisorption is stronger adsorption compared to physisorption, in which its interaction are double orders in magnitude [52]. The value of ΔH_{ads} is associated with the lower inhibition efficiency of the inhibitor as more energy is required to complete the accomplishment of the reaction [53]. At the same time, regular ΔS_{ads} shows that the solidification at a higher temperature runs slower than that at a lower temperature. As a result, more adsorbed particles were retained on the surface of metals and smoothened the surface of metals and showed constant ΔH_{ads} at all measured temperatures. This influences the protection of metals by obtaining a more thermodynamic stable adsorption process.

Atomic force microscopy measurement was carried out to evaluate the surface roughness of API 5L in 1 M HCl in the blank and non-blank solution. Fig. 7 shows a dramatic

change in corroded metal surface roughness and topography. In particular, in the blank solution, the value of an average skewness parameter was higher than that of the inhibited surface. The skewness parameter defines the ratio between the peaks and valleys where the smaller the value, the smoother the surface (Fig. 7, *b–d*). It can be reported that before adding the inhibitor, the skewness value is 0.4080 nm, which contrasts with the treated inhibitor at 0.06101 nm. This indicates that the presence of SCLE in 1 M HCl provides a denser and uniform steel surface, resulting in adequate protection of the API 5L surface. The obtained result is comparable to the previously published work [54].

Therefore, it is valuable to propose an anti-corrosion mechanism using several previous characterization results. According to the Langmuir model, the adsorption mechanism of the SCLE inhibitor on the API 5L surface involves physisorption because the value of ΔG_{ads} is closer to – 20 kJ/mol and that of ΔH_{ads} is less than 40 kJ/mol. The FTIR data reported in the previous section confirm that the functional compounds of SCLE molecules had been found on the API 5L surface. These active compounds are represented by C, OH, and N groups. In addition, the presence of alcohol, phenol, and aromatic compounds confirmed the presence of polyphenol and flavonoid components in the SCLE extract. These organic molecules are adsorbed onto the metal surface, providing a protective film and increasing corrosion inhibition. Also, the SCLE inhibitor is expected to fit the requirement to protect the API 5L metal from further metallic deterioration. This is proved by all the experimental results, which inevitably lengthens equipment life and reduces economic losses.

Despite the above, the research retains a few limitations related to applicability in determining the essential elements in corrosion products before adding inhibitors to the test solution. In this context, the X-ray diffraction (XRD) test offers the best trial related to identifying the type of corrosion product, such as the hematite of Fe_2O_3. A successful identification helps the researcher to propose a precise inhibition mechanism for the *Syzygium Cumini* leaf extract. In addition, this work remains inadequate to determine the actual elemental composition of the adsorbed metals. Using a scanning electron microscope aided by energy-dispersive X-ray spectroscopy (SEM-EDX) could facilitate overcoming the challenges. The primary benefit of the characterization is closely related to the adsorption of several functional groups identified in FTIR results onto the surface of inhibited metals.

The above difficulties disadvantage the study, especially when it attempts to determine the adsorption direction between the adsorbate and the substrate. In this case, the orientation toward the vertical direction gives a lower surface coverage area than that of the horizontal axis, as previously elaborated in [55]. In future work, a further examination of the orientation of the inhibitor paves the way to assert the obtained results in Tables 1, 2. With this in mind, the absence of the orientation study gives an uncertainty of whether the lower inhibition efficiency is related to the effect of temperature or the sharp disorientation of the inhibitor when adsorbed over the surface of metals. The modeling studies, such as the implementation of Density functional theory (DFT) and Monte Carlo simulation, realign the nature of the research. The method mentioned above intensively harnesses the atomic properties and their corresponding interaction to calculate the atomic parameter such as the energy of highest occupied molecular orbital (HOMO) and lowest unoccupied molecular orbital (LUMO). In contrast, Monte Carlo simulation helps evaluate the inhibitor molecules' lowest surface energy inclusively and their orientation on the surface of the substrate.

7. Conclusions

1. The anti-corrosion inhibition of the leaf extract was evaluated using electrochemical impedance spectroscopy and FTIR to show that the inhibitor is suitable to protect the API 5L metal from corrosion. The corrosion rate of the substrate decreased from 39.84 to 4.167 mmpy and the inhibition efficiency of SCLE increased to nearly 91 %. The EIS results demonstrate that increasing the immersion time increases the surface coverage and the inhibitor's efficiency.

2. The influence of temperature was observed to unveil the thermal stability of the inhibitor. The calculated thermodynamic result shows the adsorption process following the Langmuir model in which the nearness of the R^2 value is 1, despite the lower inhibitory capacity at an elevated temperature of 323 K.

3. The surface morphology study using AFM confirms the surface modification of an inhibitor film on the API 5L steel surface. This results in a decrease in corrosion rate from the potentiodynamic polarization, 4.167 mmpy, and η of 90 %. In addition, a more concentrated solution gives a lower skewness value of 0.061 to ensure the inhibition process, helping a smoother and more protective substrate.

Conflict of interest

The authors declare that they have no conflict of interest in relation to this research, whether financial, personal, authorship or otherwise, that could affect the research and its results presented in this paper.

Financing

The study was performed with the financial support of the Ministry of Research, Technology and Higher Education of Indonesia.

Data availability

Data will be made available on reasonable request.

Acknowledgments

The author gratefully thanks the Ministry of Research, Technology and Higher Education of Indonesia for International Indexed Publication Grants (PUTI) Q2 Financial Year of 2022–2023 Batch 3- Matching Fund (MF) Financial Year of 2022–2023, with contract number: NKB-1488/UN2.RST/HKP.05.00/2022.

References

1. Neriyana, P. S., Alva, V. D. P. (2020). A Green Approach: Evaluation of Combretum indicum (CI) Leaf Extract as an Eco-friendly Corrosion Inhibitor for Mild Steel in 1M HCl. Chemistry Africa, 3 (4), 1087–1098. doi: https://doi.org/10.1007/s42250-020-00190-z
2. Salmasifar, A., Edraki, M., Alibakhshi, E., Ramezanzadeh, B., Bahlakeh, G. (2021). Combined electrochemical/surface investigations and computer modeling of the aquatic Artichoke extract molecules corrosion inhibition properties on the mild steel surface immersed in the acidic medium. Journal of Molecular Liquids, 327, 114856. doi: https://doi.org/10.1016/j.molliq.2020.114856
3. Prifiharni, S., Mashanafie, G., Priyotomo, G., Royani, A., Ridhova, A., Elya, B., Soedarsono, J. W. (2022). Extract sarampa wood (Xylocarpus Moluccensis) as an eco-friendly corrosion inhibitor for mild steel in HCl 1M. Journal of the Indian Chemical Society, 99 (7), 100520. doi: https://doi.org/10.1016/j.jics.2022.100520
4. Abba, B. N., Idouhli, R., Ilagouma, A. T., Abouelfida, A., Khadiri, M., Romane, A. (2021). Use of Endostemon tereticaulis (Pear.) M.Ashby and Hyptis spicigera Lam. Plant Extracts as Corrosion Green Inhibitors for Mild Steel in 1M HCl: Electrochemical and Surface Morphological Studies. Protection of Metals and Physical Chemistry of Surfaces, 57 (3), 619–633. doi: https://doi.org/10.1134/s2070205121030035
5. Rajan, J. P., Shrivastava, R., Mishra, R. K. (2017). Corrosion Inhibition effect of Clerodendron Colebrookianum Walp Leaves (Phuinam) Extract on the Acid Corrosion of Mild Steel. Protection of Metals and Physical Chemistry of Surfaces, 53 (6), 1161–1172. doi: https://doi.org/10.1134/s2070205118010264
6. Sun, X., Qiang, Y., Hou, B., Zhu, H., Tian, H. (2022). Cabbage extract as an eco-friendly corrosion inhibitor for X70 steel in hydrochloric acid medium. Journal of Molecular Liquids, 362, 119733. doi: https://doi.org/10.1016/j.molliq.2022.119733
7. Fouda, A. S., El-Awady, G. Y., El Behairy, W. T. (2017). Prosopis juliflora Plant Extract as Potential Corrosion Inhibitor for Low-Carbon Steel in 1 M HCl Solution. Journal of Bio- and Tribo-Corrosion, 4 (1). doi: https://doi.org/10.1007/s40735-017-0124-x
8. Perumal, S., Muthumanickam, S., Elangovan, A., Karthik, R., kannan, R. S., Mothilal, K. K. (2017). Bauhinia tomentosa Leaves Extract as Green Corrosion Inhibitor for Mild Steel in 1M HCl Medium. Journal of Bio- and Tribo-Corrosion, 3 (2). doi: https://doi.org/10.1007/s40735-017-0072-5
9. Khadom, A. A., Abd, A. N., Ahmed, N. A., Kadhim, M. M., Fadhil, A. A. (2022). Combined influence of iodide ions and Xanthium Strumarium leaves extract as eco-friendly corrosion inhibitor for low-carbon steel in hydrochloric acid. Current Research in Green and Sustainable Chemistry, 5, 100278. doi: https://doi.org/10.1016/j.crgsc.2022.100278
10. Zakaria, F. A., Hamidon, T. S., Hussin, M. H. (2022). Applicability of winged bean extracts as organic corrosion inhibitors for reinforced steel in 0.5 M HCl electrolyte. Journal of the Indian Chemical Society, 99 (2), 100329. doi: https://doi.org/10.1016/j.jics.2021.100329
11. Raghavendra, N. (2019). Latest Exploration on Natural Corrosion Inhibitors for Industrial Important Metals in Hostile Fluid Environments: A Comprehensive Overview. Journal of Bio- and Tribo-Corrosion, 5 (3). doi: https://doi.org/10.1007/s40735-019-0240-x
12. Dehghani, A., Ghahremani, P., Mostafatabar, A. H., Ramezanzadeh, B. (2022). Plant extracts: Probable alternatives for traditional inhibitors for controlling alloys corrosion against acidic media – A review. Biomass Conversion and Biorefinery. doi: https://doi.org/10.1007/s13399-022-02893-4
13. Panchal, J., Shah, D., Patel, R., Shah, S., Prajapati, M., Shah, M. (2021). Comprehensive Review and Critical Data Analysis on Corrosion and Emphasizing on Green Eco-friendly Corrosion Inhibitors for Oil and Gas Industries. Journal of Bio- and Tribo-Corrosion, 7 (3). doi: https://doi.org/10.1007/s40735-021-00540-5
14. Chaubey, N., Savita, Qurashi, A., Chauhan, D. S., Quraishi, M. A. (2021). Frontiers and advances in green and sustainable inhibitors for corrosion applications: A critical review. Journal of Molecular Liquids, 321, 114385. doi: https://doi.org/10.1016/j.molliq.2020.114385
15. Chauhan, D. S., Quraishi, M. A., Qurashi, A. (2021). Recent trends in environmentally sustainable Sweet corrosion inhibitors. Journal of Molecular Liquids, 326, 115117. doi: https://doi.org/10.1016/j.molliq.2020.115117
16. Jmiai, A., El Ibrahimi, B., Tara, A., El Issami, S., Jbara, O., Bazzi, L. (2018). Alginate biopolymer as green corrosion inhibitor for copper in 1 M hydrochloric acid: Experimental and theoretical approaches. Journal of Molecular Structure, 1157, 408–417. doi: https://doi.org/10.1016/j.molstruc.2017.12.060
17. Kamali Ardakani, E., Kowsari, E., Ehsani, A. (2020). Imidazolium-derived polymeric ionic liquid as a green inhibitor for corrosion inhibition of mild steel in 1.0 M HCl: Experimental and computational study. Colloids and Surfaces A: Physicochemical and Engineering Aspects, 586, 124195. doi: https://doi.org/10.1016/j.colsurfa.2019.124195
18. Abaka, A. K., Ishaku, G. A., Haruna, A., Ardo, B. P. (2020). Phytochemicals Screening and Antifungal Activity of Balanites aegyptiaca Seed and Callus Extract against Candida albicans. Asian Plant Research Journal, 4 (4), 9–16. doi: https://doi.org/10.9734/aprj/2020/v4i430091
19. Fang, Y., Suganthan, B., Ramasamy, R. P. (2019). Electrochemical characterization of aromatic corrosion inhibitors from plant extracts. Journal of Electroanalytical Chemistry, 840, 74–83. doi: https://doi.org/10.1016/j.jelechem.2019.03.052
20. Fouda, A. S., Mohamed, O. A., Elabbasy, H. M. (2021). Ferula hermonis Plant Extract as Safe Corrosion Inhibitor for Zinc in Hydrochloric Acid Solution. Journal of Bio- and Tribo-Corrosion, 7 (4). doi: https://doi.org/10.1007/s40735-021-00570-z

21. Lohitkarn, J., Hemwech, P., Chantiwas, R., Jariyaboon, M. (2021). The Role of Cassava Leaf Extract as Green Inhibitor for Controlling Corrosion and Scale Problems in Cooling Water Systems. Journal of Failure Analysis and Prevention. doi: https://doi.org/10.1007/s11668-021-01121-x
22. Rustandi, A., Soedarsono, J. W., Suharno, B. (2011). The Use of Mixture of Piper Betle and Green Tea as a Green Corrosion Inhibitor for API X-52 Steel in Aerated 3.5 % NaCl Solution at Various Rotation Rates. Advanced Materials Research, 383–390, 5418–5425. doi: https://doi.org/10.4028/www.scientific.net/amr.383-390.5418
23. Huong Pham, T., Lee, W.-H., Kim, J.-G. (2022). Chrysanthemum coronarium leaves extract as an eco-friendly corrosion inhibitor for aluminum anode in aluminum-air battery. Journal of Molecular Liquids, 347, 118269. doi: https://doi.org/10.1016/j.molliq.2021.118269
24. Umoren, S. A., Solomon, M. M., Obot, I. B., Suleiman, R. K. (2021). Date palm leaves extract as a green and sustainable corrosion inhibitor for low carbon steel in 15 wt.% HCl solution: the role of extraction solvent on inhibition effect. Environmental Science and Pollution Research, 28 (30), 40879–40894. doi: https://doi.org/10.1007/s11356-021-13567-5
25. Pramana, R. I., Kusumastuti, R., Soedarsono, J. W., Rustandi, A. (2013). Corrosion Inhibition of Low Carbon Steel by Pluchea Indica Less. in 3.5% NaCL Solution. Advanced Materials Research, 785–786, 20–24. doi: https://doi.org/10.4028/www.scientific.net/amr.785-786.20
26. Wang, Q., Wu, X., Zheng, H., Xiao, X., Liu, L., Zhang, Q. et al. (2022). Insight into anti-corrosion behavior of Centipeda minima leaves extract as high-efficiency and eco-friendly inhibitor. Colloids and Surfaces A: Physicochemical and Engineering Aspects, 640, 128458. doi: https://doi.org/10.1016/j.colsurfa.2022.128458
27. Okeniyi, J. O., Ogbiye, A. S., Ogunlana, O. O., Okeniyi, E. T., Ogunlana, O. E. (2015). Investigating Solanum Aethiopicum Leaf-Extract and Sodium-Dichromate Effects on Steel-Rebar Corrosion in Saline/Marine Simulating-Environment: Implications on Sustainable Alternative for Environmentally-Hazardous Inhibitor. Engineering Solutions for Sustainability, 167–175. doi: https://doi.org/10.1007/978-3-319-48138-8_16
28. Kaban, A. P. S., Ridhova, A., Priyotomo, G., Elya, B., Maksum, A., Sadeli, Y. et al. (2021). Development of white tea extract as green corrosion inhibitor in mild steel under 1 M hydrochloric acid solution. Eastern-European Journal of Enterprise Technologies, 2 (6 (110)), 6–20. doi: https://doi.org/10.15587/1729-4061.2021.224435
29. Popoola, L. T. (2019). Organic green corrosion inhibitors (OGCIs): a critical review. Corrosion Reviews, 37 (2), 71–102. doi: https://doi.org/10.1515/corrrev-2018-0058
30. Aslam, R., Mobin, M., Aslam, J., Lgaz, H., Chung, I.-M. (2019). Inhibitory effect of sodium carboxymethylcellulose and synergistic biodegradable gemini surfactants as effective inhibitors for MS corrosion in 1 M HCl. Journal of Materials Research and Technology, 8 (5), 4521–4533. doi: https://doi.org/10.1016/j.jmrt.2019.07.065
31. Izadi, M., Shahrabi, T., Ramezanzadeh, B. (2017). Electrochemical investigations of the corrosion resistance of a hybrid sol–gel film containing green corrosion inhibitor-encapsulated nanocontainers. Journal of the Taiwan Institute of Chemical Engineers, 81, 356–372. doi: https://doi.org/10.1016/j.jtice.2017.10.039
32. Farahati, R., Mousavi-Khoshdel, S. M., Ghaffarinejad, A., Behzadi, H. (2020). Experimental and computational study of penicillamine drug and cysteine as water-soluble green corrosion inhibitors of mild steel. Progress in Organic Coatings, 142, 105567. doi: https://doi.org/10.1016/j.porgcoat.2020.105567
33. Paul Setiawan Kaban, A., Mayangsari, W., Syaiful Anwar, M., Maksum, A., Riastuti, R. et al. (2022). Experimental and modelling waste rice husk ash as a novel green corrosion inhibitor under acidic environment. Materials Today: Proceedings, 62, 4225–4234. doi: https://doi.org/10.1016/j.matpr.2022.04.738
34. Hajipour, F., Asad, S., Amoozegar, M. A., Javidparvar, A. A., Tang, J., Zhong, H., Khajeh, K. (2021). Developing a Fluorescent Hybrid Nanobiosensor Based on Quantum Dots and Azoreductase Enzyme forMethyl Red Monitoring. Iranian Biomedical Journal, 25 (1), 8–20. doi: https://doi.org/10.29252/ibj.25.1.8
35. Javidparvar, A. A., Naderi, R., Ramezanzadeh, B., Bahlakeh, G. (2019). Graphene oxide as a pH-sensitive carrier for targeted delivery of eco-friendly corrosion inhibitors in chloride solution: Experimental and theroretical investigations. Journal of Industrial and Engineering Chemistry, 72, 196–213. doi: https://doi.org/10.1016/j.jiec.2018.12.019
36. Ravari, F. B., Dadgareenezhad, A. (2013). Synergistic influence of propargyl alcohol and zinc sulfate on inhibition of corrosion of aluminum in 0.5M H2So4. Journal of the Chilean Chemical Society, 58 (3), 1853–1857. doi: https://doi.org/10.4067/s0717-97072013000300013
37. Fragoza-Mar, L., Olivares-Xometl, O., Dom nguez-Aguilar, M. A., Flores, E. A., Arellanes-Lozada, P., Jim nez-Cruz, F. (2012). Corrosion inhibitor activity of 1,3-diketone malonates for mild steel in aqueous hydrochloric acid solution. Corrosion Science, 61, 171–184. doi: https://doi.org/10.1016/j.corsci.2012.04.031
38. Hamani, H., Douadi, T., Al-Noaimi, M., Issaadi, S., Daoud, D., Chafaa, S. (2014). Electrochemical and quantum chemical studies of some azomethine compounds as corrosion inhibitors for mild steel in 1M hydrochloric acid. Corrosion Science, 88, 234–245. doi: https://doi.org/10.1016/j.corsci.2014.07.044
39. Lai, C., Xie, B., Zou, L., Zheng, X., Ma, X., Zhu, S. (2017). Adsorption and corrosion inhibition of mild steel in hydrochloric acid solution by S-allyl-O,O -dialkyldithiophosphates. Results in Physics, 7, 3434–3443. doi: https://doi.org/10.1016/j.rinp.2017.09.012
40. Godwin-Nwakwasi, E. U., Elachi, E. E., Ezeokonkwo, M. A., Onwuchuruba, L. E. (2017). A Study of the Corrosion Inhibition of Mild Steel in 0.5M Tetraoxosulphate (VI) acid by Alstonia boonei Leaves Extract as an Inhibitor at Different Temperatures.

International Journal of Advanced Engineering, Management and Science, 3 (12), 1150–1157. doi: https://doi.org/10.22161/ijaems.3.12.9

41. Hart, E. (Ed.) (2016). Corrosion inhibitors: Principles, mechanisms and applications. Nova Science Publishers, Inc.
42. Aourabi, S., Driouch, M., Sfaira, M., Mahjoubi, F., Hammouti, B., Verma, C. et al. (2021). Phenolic fraction of Ammi visnaga extract as environmentally friendly antioxidant and corrosion inhibitor for mild steel in acidic medium. Journal of Molecular Liquids, 323, 114950. doi: https://doi.org/10.1016/j.molliq.2020.114950
43. Xhanari, K., Finšgar, M., Knez Hrnčič, M., Maver, U., Knez, Ž., Seiti, B. (2017). Green corrosion inhibitors for aluminium and its alloys: a review. RSC Advances, 7 (44), 27299–27330. doi: https://doi.org/10.1039/c7ra03944a
44. Li, X., Deng, S., Fu, H., Xie, X. (2014). Synergistic inhibition effects of bamboo leaf extract/major components and iodide ion on the corrosion of steel in H3PO4 solution. Corrosion Science, 78, 29–42. doi: https://doi.org/10.1016/j.corsci.2013.08.025
45. Xu, Y. et al. (2018). Halogen-substituted pyrazolo-pyrimidine derivatives as corrosion inhibitors for copper in sulfuric acid solution. International Journal of Corrosion and Scale Inhibition, 7 (2). doi: https://doi.org/10.17675/2305-6894-2018-7-2-9
46. Kim, S., Jang, Y., Sung, S., Kim, Y. (2007). Inhibitory Activity of Phenolic Glycosides from the Fruits of Idesia polycarpa on Lipopolysaccharide-Induced Nitric Oxide Production in BV2 Microglia. Planta Medica, 73 (2), 167–169. doi: https://doi.org/10.1055/s-2006-951771
47. Shahzad, K., Sliem, M. H., Shakoor, R. A., Radwan, A. B., Kahraman, R., Umer, M. A. et al. (2020). Electrochemical and thermodynamic study on the corrosion performance of API X120 steel in 3.5% NaCl solution. Scientific Reports, 10 (1). doi: https://doi.org/10.1038/s41598-020-61139-3
48. Tan, B., Zhang, S., Qiang, Y., Li, W., Li, H., Feng, L. et al. (2020). Experimental and theoretical studies on the inhibition properties of three diphenyl disulfide derivatives on copper corrosion in acid medium. Journal of Molecular Liquids, 298, 111975. doi: https://doi.org/10.1016/j.molliq.2019.111975
49. Sedik, A., Lerari, D., Salci, A., Athmani, S., Bachari, K., Gecibesler, . H., Solmaz, R. (2020). Dardagan Fruit extract as eco-friendly corrosion inhibitor for mild steel in 1 M HCl: Electrochemical and surface morphological studies. Journal of the Taiwan Institute of Chemical Engineers, 107, 189–200. doi: https://doi.org/10.1016/j.jtice.2019.12.006
50. Miralrio, A., Espinoza Vázquez, A. (2020). Plant Extracts as Green Corrosion Inhibitors for Different Metal Surfaces and Corrosive Media: A Review. Processes, 8 (8), 942. doi: https://doi.org/10.3390/pr8080942
51. Ricky, E. X., Mpelwa, M., Xu, X. (2021). The study of m-pentadecylphenol on the inhibition of mild steel corrosion in 1 M HCl solution. Journal of Industrial and Engineering Chemistry, 101, 359–371. doi: https://doi.org/10.1016/j.jiec.2021.05.047
52. Al-Ghouti, M. A., Da'ana, D. A. (2020). Guidelines for the use and interpretation of adsorption isotherm models: A review. Journal of Hazardous Materials, 393, 122383. doi: https://doi.org/10.1016/j.jhazmat.2020.122383
53. Vashishth, P., Bairagi, H., Narang, R., Shukla, S. K., Mangla, B. (2022). Thermodynamic and electrochemical investigation of inhibition efficiency of green corrosion inhibitor and its comparison with synthetic dyes on MS in acidic medium. Journal of Molecular Liquids, 365, 120042. doi: https://doi.org/10.1016/j.molliq.2022.120042
54. Noorbakhsh Nezhad, A. H., Davoodi, A., Mohammadi Zahrani, E., Arefinia, R. (2020). The effects of an inorganic corrosion inhibitor on the electrochemical behavior of superhydrophobic micro-nano structured Ni films in 3.5% NaCl solution. Surface and Coatings Technology, 395, 125946. doi: https://doi.org/10.1016/j.surfcoat.2020.125946
55. Chauhan, D. S., Quraishi, M. A., Srivastava, V., Haque, J., ibrahimi, B. E. (2021). Virgin and chemically functionalized amino acids as green corrosion inhibitors: Influence of molecular structure through experimental and in silico studies. Journal of Molecular Structure, 1226, 129259. doi: https://doi.org/10.1016/j.molstruc.2020.129259